

# Crystal Growth, Structural and Thermal Studies of $\text{FeC}_4\text{H}_4\text{O}_6 \cdot 2.5\text{H}_2\text{O}$

Takanori Fukami<sup>1</sup>, Shuta Tahara<sup>1</sup>

<sup>1</sup>Department of Physics and Earth Sciences, Faculty of Science, University of the Ryukyus, Japan

Correspondence: Takanori Fukami, Department of Physics and Earth Sciences, Faculty of Science, University of the Ryukyus, Okinawa 903-0213, Japan.

Received: May 11, 2022 Accepted: June 27, 2022 Online Published: July 4, 2022

doi:10.5539/ijc.v14n2p8

URL: <https://doi.org/10.5539/ijc.v14n2p8>

## Abstract

Single crystals of iron(II) tartrate hemi-pentahydrate,  $\text{FeC}_4\text{H}_4\text{O}_6 \cdot 2.5\text{H}_2\text{O}$ , were grown by the gel method using silica gels. Differential scanning calorimetry, thermogravimetric-differential thermal analysis, and X-ray diffraction measurements were performed on the single crystals. The space group symmetry (orthorhombic  $P2_12_12_1$ ) and structural parameters were determined at room temperature. The crystal structure consisted of slightly distorted  $\text{FeO}_6$  octahedra,  $\text{C}_4\text{H}_4\text{O}_6$  and  $\text{H}_2\text{O}$  molecules,  $\text{C}_4\text{H}_4\text{O}_6\text{-Fe-C}_4\text{H}_4\text{O}_6$  chains jointed by Fe-O bonds, and O-H $\cdots$ O hydrogen-bonding frameworks between adjacent molecules. Weight losses due to thermal decomposition of the crystal were found to occur in the temperature range of 300–1060 K. We inferred that the weight losses were caused by the evaporation of bound water molecules and the evolution of  $\text{H}_2\text{CO}$ , CO, and  $\text{O}_2$  gases from  $\text{C}_4\text{H}_4\text{O}_6$  molecules, and that the black residue after decomposition was composed of triiron tetraoxide ( $\text{Fe}_3\text{O}_4$ ) and carbon.

**Keywords:**  $\text{FeC}_4\text{H}_4\text{O}_6 \cdot 2.5\text{H}_2\text{O}$ , crystal structure, thermal decomposition, X-ray diffraction, TG-DTA

## 1. Introduction

Tartrate compounds are formed by the reaction of tartaric acid with compounds containing positive ions (i.e., two monovalent cations or one divalent cation) (Desai & Patel, 1988; Fukami & Tahara, 2018; Fukami & Tahara, 2020; Fukami & Tahara, 2021; Labutina, Marychev, Portnov, Somov, & Chuprunov, 2011). Tartaric acid ( $\text{C}_4\text{H}_6\text{O}_6$ ; systematic name: 2,3-dihydroxybutanedioic acid) has two chiral carbon atoms in its structure, which provides the possibility for four different forms of chiral, racemic, and achiral isomers: L(+)-tartaric, D(–)-tartaric, racemic (DL-) tartaric, and meso-tartaric acid (Bootsma & Schoone, 1967; Fukami, Tahara, Yasuda, & Nakasone, 2016; Song, Teng, Dong, Ma, & Sun, 2006). Some of these compounds are of interest in research because of their physical properties, particularly their excellent dielectric, ferroelectric, piezoelectric, and nonlinear optical properties (Abdel-Kader et al., 1991; Firdous, Quasim, Ahmad, & Kotru, 2010; Torres et al., 2002). Moreover, they were formerly used in various industrial applications, for example as transducers and mechanical devices.

Various experimental studies on iron tartrate crystals have been conducted by many researchers (Dhikale, Shitole, Nahire, & Chavan, 2019; Joseph, Joshi, & Joshi, 1997; Kachi, 1974; Labutina, Marychev, Portnov, Somov, & Chuprunov, 2011; Mathivanan, Haris, & Pramana, 2013; Venkataraman, Mukhedkar, & Mukhedkar, 1989). These studies include the crystal growth, and investigation of structural, thermal, electrical, and optical properties of pure and copper-doped iron tartrate crystals. The thermogravimetric analysis conducted by Venkataraman et al. (Venkataraman, Mukhedkar, & Mukhedkar, 1989) implied that the pure iron tartrate crystal is reduced to  $\alpha$ -iron(III) oxide ( $\alpha\text{-Fe}_2\text{O}_3$ ) by thermal decomposition, and by Joseph et al. (Joseph, Joshi, & Joshi, 1997) suggested that it is reduced to iron(II) oxide (FeO). Furthermore, powder X-ray diffraction (XRD) patterns showed that the crystal is orthorhombic with lattice constants of  $a = 9.8845 \text{ \AA}$ ,  $b = 7.4420 \text{ \AA}$ , and  $c = 8.8480 \text{ \AA}$  (Venkataraman, Mukhedkar, & Mukhedkar, 1989). These physical properties were measured on iron tartrate crystals comprising polycrystalline aggregates. Labutina et al. (Labutina, Marychev, Portnov, Somov, & Chuprunov, 2011) have grown many tartrate single crystals by the gel method, and determined the crystal system and lattice parameters (lattice constants and angles). The  $\text{FeC}_4\text{H}_4\text{O}_6 \cdot 2.5\text{H}_2\text{O}$  crystal was orthorhombic with space group  $P2_12_12_1$  and lattice constants  $a = 7.8838(2) \text{ \AA}$ ,  $b = 11.2778(4) \text{ \AA}$ , and  $c = 18.3476(6) \text{ \AA}$ . Kachi (Kachi, 1974) has reported the growth of tartrate compounds by the gel method using silica gels. The photographs of single and aggregate  $\text{FeC}_4\text{H}_4\text{O}_6$  crystals were presented in the paper.

The purpose of this paper is to report the growth of single  $\text{FeC}_4\text{H}_4\text{O}_6 \cdot 2.5\text{H}_2\text{O}$  crystals by the gel method, and to determine the crystal structure using single-crystal X-ray diffraction. Moreover, the thermal properties of the crystal are studied by means of differential scanning calorimetry (DSC) and thermogravimetric-differential thermal analysis (TG-DTA).

## 2. Experimental

### 2.1 Crystal Growth

The  $\text{FeC}_4\text{H}_4\text{O}_6 \cdot 2.5\text{H}_2\text{O}$  crystals were grown at room temperature by the gel method using silica gels. The gels were prepared in test tubes (length of 200 mm and diameter of 30 mm) using aqueous solutions of  $\text{Na}_2\text{SiO}_3$  (20 ml of 1.0 M),  $\text{C}_4\text{H}_6\text{O}_6$  (25 ml of 0.5 M), and  $\text{CH}_3\text{COOH}$  (25 ml of 2.0 M), and aged for seven days. Thereafter, a solution of  $\text{FeCl}_3 \cdot 6\text{H}_2\text{O}$  (30 ml of 0.25 M) was gently poured on top of the gel. The crystals were harvested after approximately 16 months. Figure 1 shows a photograph of single crystals and polycrystalline aggregates of  $\text{FeC}_4\text{H}_4\text{O}_6 \cdot 2.5\text{H}_2\text{O}$ . Single crystals were grown on the gel surface in the  $\text{FeCl}_3$  solution, and polycrystalline aggregates were grown in the gel medium and on the surface. The external forms of single crystals are similar to that reported in the previous paper (Kachi, 1974). The polycrystalline aggregates, which are quasi-spherical in shape and brown in color, are also very similar to those reported by Dhikale et al. (Dhikale, Shitole, Nahire, & Chavan, 2019) and by Mathivanan et al. (Mathivanan & Haris, 2013).

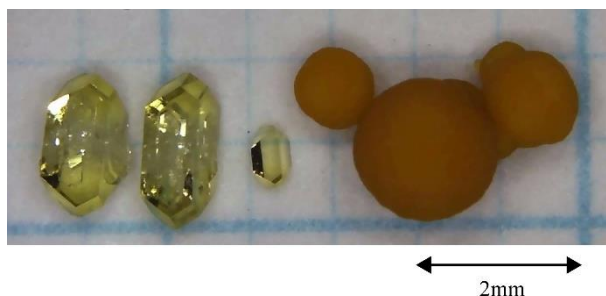


Figure 1. Photograph of single and polycrystalline  $\text{FeC}_4\text{H}_4\text{O}_6 \cdot 2.5\text{H}_2\text{O}$  crystals

### 2.2 X-ray Measurements

The X-ray diffraction measurements were performed using a Rigaku Saturn CCD X-ray diffractometer with graphite-monochromated  $\text{Mo } K_\alpha$  radiation ( $\lambda = 0.71073 \text{ \AA}$ ). Single-crystal diffraction data for the  $\text{FeC}_4\text{H}_4\text{O}_6 \cdot 2.5\text{H}_2\text{O}$  crystal were collected at 299 K using an  $\omega$  scan mode with a crystal-to-detector distance of 40 mm, and processed using the CrystalClear software package. The intensity data were corrected for Lorentz polarization and absorption effects. The crystal structure was solved by direct methods using the SIR2014 program and refined on  $F^2$  by full-matrix least-squares methods using the SHELXL-2017 program in the WinGX package (Burla et al., 2015; Farrugia, 2012; Sheldrick, 2015).

### 2.3 Thermal Measurements

DSC and TG-DTA measurements were respectively carried out in the temperature ranges of 100–315 K and 300–1320 K, using DSC7020 and TG-DTA7300 systems from Seiko Instruments Inc. Aluminium (for DSC) and platinum (for TG-DTA) open pans were used as measuring vessels. Fine powder samples, prepared by grinding several pieces of single crystals, were used for the thermal measurements.

## 3. Results and Discussion

### 3.1 Structure Determination

The crystal structure of  $\text{FeC}_4\text{H}_4\text{O}_6 \cdot 2.5\text{H}_2\text{O}$  was determined at room temperature. The lattice parameters calculated from all observed X-ray reflections showed that the crystal belongs to an orthorhombic system, and the systematic extinctions indicated that its space group is  $P2_12_12_1$ . The obtained lattice parameters are similar to those reported by Labutina et al. (Labutina, Marychev, Portnov, Somov, & Chuprunov, 2011). All non-hydrogen atoms were refined anisotropically, and hydrogen atoms were located on difference electron density maps and refined isotropically. The positional and thermal parameters for four H atoms belonging to water molecules, which did not converge to reasonable values, were fixed during the refinement. A final  $R$ -factor of 3.55% was calculated for 7158 unique observed reflections.

The relevant crystal data, and a summary of the intensity data collection and structure refinement are given in Table 1. Figure 2 shows the projection along the  $a$ -axis of the  $\text{FeC}_4\text{H}_4\text{O}_6 \cdot 2.5\text{H}_2\text{O}$  structure. The positional parameters in fractions of the unit cell and thermal parameters are listed in Table 2. Selected bond lengths and angles are given in Table 3, and hydrogen-bond geometries are presented in Table 4.

Table 1. Crystal data, intensity data collections, and structure refinements for FeC<sub>4</sub>H<sub>4</sub>O<sub>6</sub>·2.5H<sub>2</sub>O

Compound, $M_r$	Fe <sub>2</sub> O <sub>17</sub> C <sub>8</sub> H <sub>18</sub> , 497.92
Measurement temperature	299 K
Crystal system, space group	Orthorhombic, $P2_12_12_1$
Lattice constants	$a = 7.8905(3) \text{ \AA}$ , $b = 11.3004(3) \text{ \AA}$ $c = 18.3888(6) \text{ \AA}$
$V$ , $Z$	$1639.65(9) \text{ \AA}^3$ , 4
$D(\text{cal.})$ , $\mu(\text{Mo } K\alpha)$ , $F(000)$	$2.017 \text{ Mg}\cdot\text{m}^{-3}$ , $1.863 \text{ mm}^{-1}$ , 1016
Crystal size	$0.14 \times 0.18 \times 0.22 \text{ mm}^3$
$\theta$ range for data collection	$2.12\text{--}35.00^\circ$
Index ranges	$-12 \leq h \leq 12$ , $-18 \leq k \leq 18$ , $-29 \leq l \leq 29$
Reflections collected, unique	42812, 7224 [ $R(\text{int}) = 0.0326$ ]
Completeness to $\theta_{\text{max}}$	99.9%
Absorption correction type	Numerical
Transmission factor $T_{\text{min}}\text{--}T_{\text{max}}$	0.7004–0.7756
Date, parameter	7158 [ $I > 2\sigma(I)$ ], 301
Final $R$ indices	$R_1 = 0.0355$ , $wR_2 = 0.0717$
$R$ indices (all data)	$R_1 = 0.0360$ , $wR_2 = 0.0720$
Weighting scheme	$w = 1/[\sigma^2(F_o^2) + (0.0245P)^2 + 0.8541P]$ $P = (F_o^2 + 2F_c^2)/3$
Flack parameter	-0.009(4)
Goodness-of-fit on $F^2$	1.105
Extinction coefficient	0.0029(4)
Largest diff. peak and hole	0.454 / -0.518 e $\text{\AA}^{-3}$

### 3.2 Structure Description

The obtained unit cell structure of FeC<sub>4</sub>H<sub>4</sub>O<sub>6</sub>·2.5H<sub>2</sub>O comprises two non-equivalent Fe atoms, two crystallographically independent C<sub>4</sub>H<sub>4</sub>O<sub>6</sub> molecules, and five independent H<sub>2</sub>O molecules. Figure 2 shows that the C<sub>4</sub>H<sub>4</sub>O<sub>6</sub> molecules are arranged periodically along the  $c$ -axis, and the Fe atoms are located between the C<sub>4</sub>H<sub>4</sub>O<sub>6</sub> molecules. Furthermore, the Fe atoms are bonded to six nearest-neighboring O atoms, forming slightly distorted FeO<sub>6</sub> octahedra, as listed in Table 3. The six O atoms include five O atoms from three C<sub>4</sub>H<sub>4</sub>O<sub>6</sub> molecules and one O atom from the H<sub>2</sub>O molecule. Therefore, the three C<sub>4</sub>H<sub>4</sub>O<sub>6</sub> molecules and one H<sub>2</sub>O molecule are connected to each other through the Fe–O bonds. The lengths of the Fe–O bonds are in the range of 2.060(2)–2.188(2) Å, and the average Fe–O distance is 2.117 Å. As shown in Table 4 and Fig. 2, the C<sub>4</sub>H<sub>4</sub>O<sub>6</sub> and H<sub>2</sub>O molecules are connected by O–H···O hydrogen bonds, and zigzag hydrogen-bonded chains are formed in the  $ab$ -planes (in the  $(1/4)c$ - and  $(3/4)c$ -planes). No hydrogen-bonded chains exist along the  $c$ -axis. However, C<sub>4</sub>H<sub>4</sub>O<sub>6</sub>–Fe–C<sub>4</sub>H<sub>4</sub>O<sub>6</sub> chains jointed by the Fe–O bonds run along the  $c$ -axis.

The lengths of six O–C and four C–C bonds in the C<sub>4</sub>H<sub>4</sub>O<sub>6</sub> molecules of FeC<sub>4</sub>H<sub>4</sub>O<sub>6</sub>·2.5H<sub>2</sub>O are similar to those of other tartrate crystals mentioned in our previous studies (Fukami & Tahara, 2018; Fukami & Tahara, 2020). The comparison of these bond lengths shows that the two O–C bonds of hydroxyl groups in this crystal have single-bond character, the remaining four bonds have double-bond character, and all the C–C bonds have single-bond character. The angles between the two least-squares planes of atoms, [C(1)C(2)O(1)O(2)O(3) and C(3)C(4)O(4)O(5)O(6)], and [C(5)C(6)O(7)O(8)O(9) and C(7)C(8)O(10)O(11)O(12)], in the C<sub>4</sub>H<sub>4</sub>O<sub>6</sub> molecules were calculated to be 49.90(8)° and 72.15(7)°, respectively. These angles are similar to those of L-MnC<sub>4</sub>H<sub>4</sub>O<sub>6</sub>·2H<sub>2</sub>O (58.0(1)° and 74.6(1)°) and DL-MnC<sub>4</sub>H<sub>4</sub>O<sub>6</sub>·2H<sub>2</sub>O (51.39(3)° and 65.71(4)°) crystals in the previous study (Fukami & Tahara, 2020).

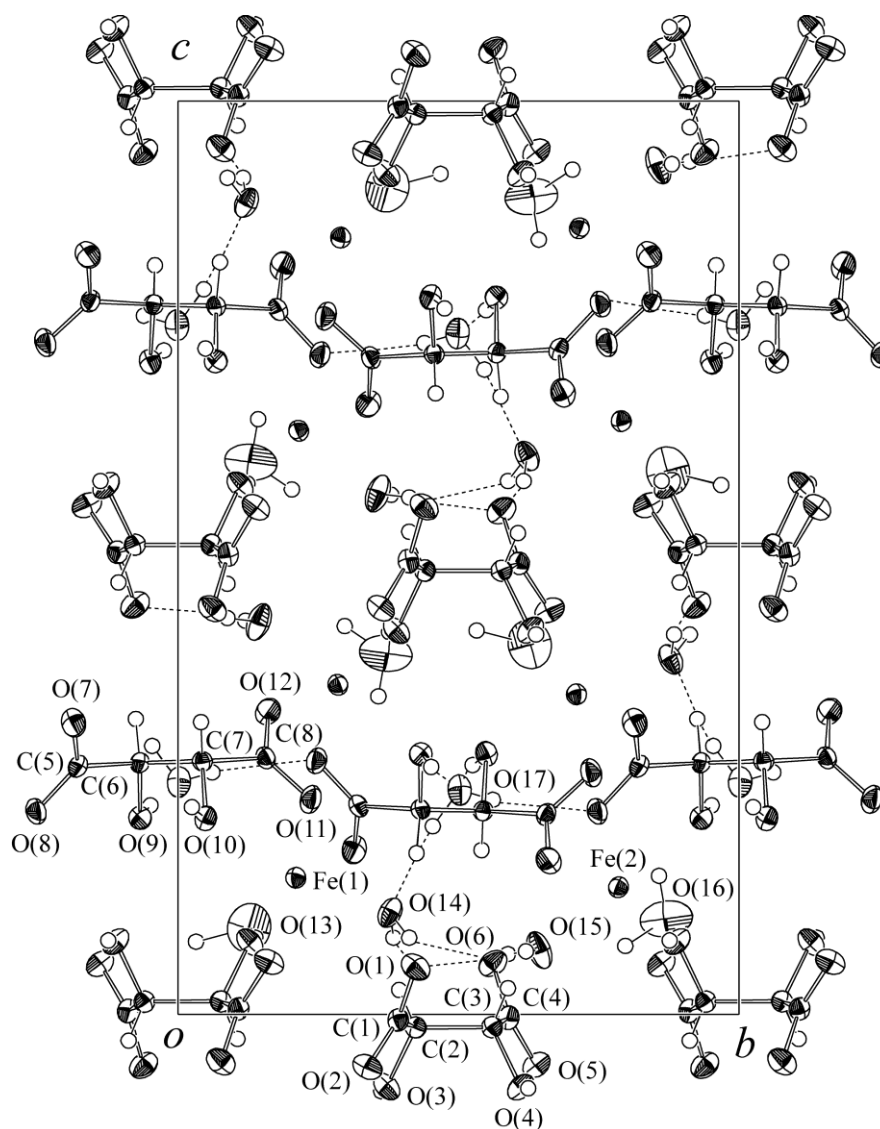


Figure 2. ORTEP projection along the  $a$ -axis of  $\text{FeC}_4\text{H}_4\text{O}_6 \cdot 2.5\text{H}_2\text{O}$  structure at room temperature, with 50% probability-displacement thermal ellipsoids

The solid and dashed short lines indicate O-H...O hydrogen bonds listed in Table 4.

Table 2. Atomic coordinates and thermal parameters ( $\times 10^4 \text{ \AA}^2$ ) for  $\text{FeC}_4\text{H}_4\text{O}_6 \cdot 2.5\text{H}_2\text{O}$  at room temperature, with standard deviations in parentheses. The anisotropic thermal parameters are defined as  $\exp[-2\pi^2(U_{11}a^*h^2 + U_{22}b^*k^2 + U_{33}c^*l^2 + 2U_{23}b^*c^*kl + 2U_{13}a^*c^*hl + 2U_{12}a^*b^*hk)]$ . The isotropic thermal parameters ( $\text{\AA}^2$ ) for H atoms are listed under  $U_{11}$

Atom	<i>x</i>	<i>y</i>	<i>z</i>	$U_{11}$	$U_{22}$	$U_{33}$	$U_{23}$	$U_{13}$	$U_{12}$
Fe(1)	0.87904(4)	0.21011(3)	0.14954(2)	190(1)	171(1)	188(1)	-1(1)	4(1)	-10(1)
Fe(2)	0.60234(4)	0.78487(3)	0.13919(2)	190(1)	168(1)	188(1)	12(1)	-7(1)	-10(1)
C(1)	0.4409(3)	0.3922(2)	-0.0061(1)	179(9)	185(9)	219(10)	6(7)	-32(7)	26(7)
C(2)	0.2539(3)	0.4235(2)	-0.0142(1)	158(8)	192(9)	193(9)	-3(7)	-6(7)	24(7)
C(3)	0.2321(3)	0.5597(2)	-0.0140(1)	167(9)	185(9)	201(9)	0(7)	8(7)	28(7)
C(4)	0.0451(3)	0.5894(2)	-0.0038(1)	165(9)	181(9)	245(10)	11(8)	28(7)	10(7)
C(5)	0.7985(3)	-0.1783(2)	0.2718(1)	196(9)	161(8)	209(9)	37(7)	-16(7)	15(7)
C(6)	0.6858(3)	-0.0680(2)	0.2755(1)	188(9)	154(8)	172(9)	9(7)	-1(7)	22(7)
C(7)	0.7968(3)	0.0436(2)	0.2771(1)	176(9)	171(8)	169(9)	-4(7)	3(7)	22(7)
C(8)	0.6892(3)	0.1560(2)	0.2809(1)	211(9)	160(8)	207(9)	-28(7)	23(8)	14(7)
O(1)	0.5098(3)	0.4236(2)	0.0517(1)	262(9)	349(10)	299(10)	-85(8)	-113(8)	87(8)
O(2)	0.5130(2)	0.3377(2)	-0.0576(1)	180(8)	368(10)	264(9)	-76(7)	-25(7)	79(7)
O(3)	0.1928(2)	0.3720(2)	-0.0792(1)	169(7)	297(9)	298(9)	-102(7)	-43(6)	24(7)
O(4)	0.2886(2)	0.6106(2)	-0.0797(1)	165(7)	294(9)	291(9)	101(7)	50(6)	24(6)
O(5)	-0.0338(2)	0.6388(2)	-0.0553(1)	161(7)	321(9)	279(9)	83(8)	22(6)	33(7)
O(6)	-0.0187(3)	0.5612(2)	0.0557(1)	269(9)	332(10)	287(9)	84(8)	104(7)	62(8)
O(7)	0.9099(3)	-0.1861(2)	0.3194(1)	320(10)	252(8)	346(9)	-27(7)	-156(8)	85(7)
O(8)	0.7709(3)	-0.2530(2)	0.2223(1)	350(10)	174(7)	282(9)	-35(6)	-99(7)	66(7)
O(9)	0.5724(2)	-0.0674(2)	0.2150(1)	177(7)	225(7)	223(7)	-6(6)	-39(6)	34(6)
O(10)	0.9048(2)	0.0496(2)	0.2147(1)	196(7)	204(7)	263(8)	21(6)	59(7)	33(6)
O(11)	0.7158(3)	0.2364(2)	0.2355(1)	407(11)	188(8)	334(10)	47(7)	142(8)	83(7)
O(12)	0.5843(3)	0.1606(2)	0.3316(1)	368(10)	267(8)	296(9)	42(7)	152(8)	110(8)
O(13)	0.3589(3)	0.1269(3)	0.0948(2)	217(11)	800(22)	1007(25)	58(20)	47(14)	53(13)
O(14)	0.8028(3)	0.3779(2)	0.1113(1)	213(8)	248(8)	365(10)	92(8)	-67(7)	-13(7)
O(15)	0.6673(3)	0.6440(2)	0.0704(2)	256(10)	271(9)	578(14)	-149(10)	106(10)	-5(8)
O(16)	0.1220(4)	0.8703(4)	0.1047(2)	314(13)	1177(28)	555(16)	89(19)	23(13)	192(16)
O(17)	0.7583(3)	0.5018(2)	0.2456(1)	337(11)	236(9)	410(12)	-12(9)	-20(9)	14(8)
H(1)	0.199(4)	0.394(3)	0.027(2)	0.028(9)					
H(2)	0.282(4)	0.588(3)	0.029(2)	0.022(8)					
H(3)	0.618(4)	-0.075(3)	0.324(2)	0.023(8)					
H(4)	0.870(5)	0.041(3)	0.320(2)	0.04(1)					
H(5)	0.065(6)	0.362(4)	-0.084(2)	0.05(1)					
H(6)	0.397(5)	0.624(4)	-0.081(2)	0.04(1)					
H(7)	0.465(6)	-0.049(4)	0.229(2)	0.05(1)					
H(8)	1.006(6)	0.025(4)	0.227(2)	0.04(1)					
H(9)	0.305	0.032	0.080	0.07					
H(10)	0.259	0.158	0.056	0.07					
H(11)	0.877(6)	0.412(4)	0.084(2)	0.06(1)					
H(12)	0.703(6)	0.384(4)	0.084(2)	0.06(2)					
H(13)	0.757(7)	0.620(4)	0.069(3)	0.07(2)					
H(14)	0.604(5)	0.588(3)	0.066(2)	0.04(1)					
H(15)	0.139	0.857	0.152	0.07					
H(16)	0.174	0.797	0.075	0.07					
H(17)	0.758(7)	0.561(5)	0.235(3)	0.07(2)					
H(18)	0.764(6)	0.454(4)	0.206(3)	0.07(2)					

Table 3. Selected interatomic distances ( $\text{\AA}$ ) and angles (degrees) for  $\text{FeC}_4\text{H}_4\text{O}_6 \cdot 2.5\text{H}_2\text{O}$ 

Fe(1)–O(2) <sup>(1)</sup>	2.066(2)	Fe(1)–O(3) <sup>(1)</sup>	2.167(2)
Fe(1)–O(7) <sup>(2)</sup>	2.115(2)	Fe(1)–O(10)	2.183(2)
Fe(1)–O(11)	2.060(2)	Fe(1)–O(14)	2.110(2)
Fe(2)–O(4) <sup>(3)</sup>	2.180(2)	Fe(2)–O(5) <sup>(3)</sup>	2.067(2)
Fe(2)–O(8) <sup>(4)</sup>	2.071(2)	Fe(2)–O(9) <sup>(4)</sup>	2.188(2)
Fe(2)–O(12) <sup>(2)</sup>	2.105(2)	Fe(2)–O(15)	2.097(2)
O(1)–C(1)	1.245(3)	O(2)–C(1)	1.265(3)
O(3)–C(2)	1.413(3)	O(4)–C(3)	1.411(3)
O(5)–C(4)	1.264(3)	O(6)–C(4)	1.246(3)
O(7)–C(5)	1.244(3)	O(8)–C(5)	1.259(3)
O(9)–C(6)	1.428(3)	O(10)–C(7)	1.432(3)
O(11)–C(8)	1.252(3)	O(12)–C(8)	1.247(3)
C(1)–C(2)	1.524(3)	C(2)–C(3)	1.549(3)
C(3)–C(4)	1.525(3)	C(5)–C(6)	1.532(3)
C(6)–C(7)	1.535(3)	C(7)–C(8)	1.530(3)
O(1)–C(1)–O(2)	125.5(2)	O(1)–C(1)–C(2)	116.2(2)
O(2)–C(1)–C(2)	118.3(2)	O(3)–C(2)–C(1)	108.5(2)
O(3)–C(2)–C(3)	111.9(2)	O(4)–C(3)–C(2)	111.6(2)
O(4)–C(3)–C(4)	108.8(2)	O(5)–C(4)–O(6)	125.0(2)
O(5)–C(4)–C(3)	118.7(2)	O(6)–C(4)–C(3)	116.3(2)
O(7)–C(5)–O(8)	125.6(2)	O(7)–C(5)–C(6)	115.9(2)
O(8)–C(5)–C(6)	118.5(2)	O(9)–C(6)–C(5)	109.4(2)
O(9)–C(6)–C(7)	111.6(2)	O(10)–C(7)–C(6)	111.3(2)
O(10)–C(7)–C(8)	109.1(2)	O(11)–C(8)–O(12)	125.4(2)
O(11)–C(8)–C(7)	118.6(2)	O(12)–C(8)–C(7)	115.9(2)
C(1)–C(2)–C(3)	109.7(2)	C(2)–C(3)–C(4)	109.1(2)
C(5)–C(6)–C(7)	109.8(2)	C(6)–C(7)–C(8)	111.5(2)

Symmetry codes: (1)  $x+1/2, -y+1/2, -z$ ; (2)  $-x+1, y+1/2, -z+1/2$ ; (3)  $x+1/2, -y+3/2, -z$ ; (4)  $x, y+1, z$ .

Table 4. Hydrogen bond distances ( $\text{\AA}^2$ ) and angles (degrees) for  $\text{FeC}_4\text{H}_4\text{O}_6 \cdot 2.5\text{H}_2\text{O}$ 

D–H $\cdots$ A	D–H	H $\cdots$ A	D $\cdots$ A	$\angle$ D–H $\cdots$ A
C(2)–H(1) $\cdots$ O(2) <sup>(1)</sup>	0.93(3)	3.05(3)	3.750(3)	133(3)
C(3)–H(2) $\cdots$ O(12) <sup>(2)</sup>	0.94(3)	2.90(3)	3.827(3)	174(3)
C(6)–H(3) $\cdots$ O(1) <sup>(3)</sup>	1.03(3)	2.51(3)	3.534(3)	172(3)
C(7)–H(4) $\cdots$ O(6) <sup>(3)</sup>	0.98(4)	2.58(4)	3.543(3)	169(3)
O(3)–H(5) $\cdots$ O(13) <sup>(4)</sup>	1.02(4)	1.64(4)	2.650(3)	169(4)
O(4)–H(6) $\cdots$ O(16) <sup>(4)</sup>	0.87(4)	1.83(4)	2.679(3)	166(4)
O(9)–H(7) $\cdots$ O(17) <sup>(3)</sup>	0.91(5)	1.91(5)	2.818(3)	175(4)
O(10)–H(8) $\cdots$ O(17) <sup>(5)</sup>	0.88(4)	1.94(5)	2.809(3)	169(4)
O(13)–H(9) $\cdots$ O(5) <sup>(6)</sup>		2.356(2)	3.203(4)	126.3(1)
O(13)–H(9) $\cdots$ O(16) <sup>(7)</sup>	1.184(4)	2.376(4)	3.454(6)	150.2(2)
O(13)–H(10) $\cdots$ O(2) <sup>(4)</sup>	1.111(3)	1.945(2)	2.843(3)	135.1(2)
O(14)–H(11) $\cdots$ O(6) <sup>(8)</sup>	0.86(5)	1.95(5)	2.705(3)	147(4)
O(14)–H(12) $\cdots$ O(1)	0.94(5)	1.69(5)	2.611(3)	165(5)
O(15)–H(13) $\cdots$ O(6) <sup>(8)</sup>	0.76(5)	1.90(5)	2.663(3)	175(5)
O(15)–H(14) $\cdots$ O(1)	0.81(4)	2.02(4)	2.805(3)	163(4)
O(16)–H(15) $\cdots$ O(11) <sup>(2)</sup>		2.737(2)	3.545(4)	152.2(2)
O(16)–H(15) $\cdots$ O(17) <sup>(2)</sup>	0.887(3)	2.626(2)	3.267(4)	130.0(3)
O(16)–H(16) $\cdots$ O(6)	1.074(4)	3.089(2)	3.775(5)	122.4(2)
O(17)–H(17) $\cdots$ O(8) <sup>(9)</sup>	0.70(5)	2.12(5)	2.807(3)	170(6)
O(17)–H(18) $\cdots$ O(14)	0.91(5)	1.97(5)	2.860(3)	168(5)

Symmetry codes: (1)  $x-1/2, -y+1/2, -z$ ; (2)  $-x+1, y+1/2, -z+1/2$ ; (3)  $-x+1, y-1/2, -z+1/2$ ; (4)  $x+1/2, -y+3/2, -z$ ; (5)  $-x+2, y-1/2, -z+1/2$ ; (6)  $x+1/2, -y+1/2, -z$ ; (7)  $x, y-1, z$ ; (8)  $x+1, y, z$ ; (9)  $x, y+1, z$ .

### 3.3 Thermal Analysis

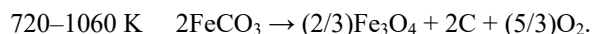
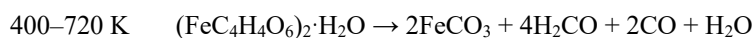
Figure 3 shows the TG, differential TG (DTG), and DTA curves in the temperature range of 300–1320 K for the  $\text{FeC}_4\text{H}_4\text{O}_6 \cdot 2.5\text{H}_2\text{O}$  crystal. These analyses were performed at a heating rate of  $10 \text{ K} \cdot \text{min}^{-1}$  under a dry nitrogen gas flow of  $300 \text{ ml} \cdot \text{min}^{-1}$ . The sample weight was 5.56 mg. The observed TG curve is remarkably similar to that in the previous papers (Joseph, Joshi & Joshi, 1997; Venkataraman, Mukhedkar, & Mukhedkar, 1989). The DTA curve shows four endothermic peaks at 350, 616, 674, and 971 K including a small peak, and the DTG curve shows four peaks at 349, 629, 649, and 969 K. These results indicate that the DTA peaks correspond relatively closely to the DTG peaks. The DTG curve, which is the first derivative of TG curve, reveals the temperature dependence of weight loss rate due to thermal decomposition of sample. Therefore, the DTA peaks are associated with the maximum rate of weight loss in the TG curve. DSC measurements on the powdered sample (5.42 mg) of  $\text{FeC}_4\text{H}_4\text{O}_6 \cdot 2.5\text{H}_2\text{O}$  were performed in the temperature range from 100 to 315 K with a heating rate of  $10 \text{ K} \cdot \text{min}^{-1}$ . No obvious endothermic or exothermic peaks were observed in the DSC curve, except for the change in the slope of the baseline due to the endothermic peak at 350 K. Generally, it is believed that a clear peak in the DSC curve is attributed to the change in the exchange energy at phase transition. Thus, the obtained result indicates that there is no phase transition in the temperature range of 100–315 K for the  $\text{FeC}_4\text{H}_4\text{O}_6 \cdot 2.5\text{H}_2\text{O}$  crystal.

Three discrete weight losses in the TG curve were observed at approximately 350, 620, and 970 K. The weight loss rates in the temperature ranges of 300–400, 400–720, and 720–1060 K were 14.9, 38.6, and 7.8%, respectively. Table 5 shows the experimental and theoretical weight losses in each temperature range. The theoretical weight losses were calculated based on the following considerations.

Table 5. TG results for thermal decomposition of  $\text{FeC}_4\text{H}_4\text{O}_6 \cdot 2.5\text{H}_2\text{O}$ 

Temp. range [K]	Weight loss (obs.) [%]	Weight loss (cal.) [%]	Elimination molecules
300–400	14.9	14.5	$4\text{H}_2\text{O}$
400–720	38.6	39.0	$4\text{H}_2\text{CO}$ , $2\text{CO}$ , $\text{H}_2\text{O}$
720–1060	7.8	10.7	$(5/3)\text{O}_2$
Total	61.3	64.2	

The weight losses in the TG curve of  $\text{FeC}_4\text{H}_4\text{O}_6 \cdot 2.5\text{H}_2\text{O}$  may be caused by the evaporation of bound water molecules and the evolution of gases from the sample, similarly to our previous studies (Fukami & Tahara, 2018; Fukami & Tahara, 2020; Fukami & Tahara, 2021). The unit cell of the crystal contains two crystallographically independent formula units, and its chemical formula is expressed as  $(\text{FeC}_4\text{H}_4\text{O}_6)_2 \cdot 5\text{H}_2\text{O}$ . Therefore, the theoretical weight losses due to the thermal decomposition were calculated using the formula weight  $M=497.92 \text{ g}\cdot\text{mol}^{-1}$ , as listed in Table 2. Presumably, the elimination of bound water molecules from the crystal occurs with increasing temperature from room temperature. Above 400 K, the evolution of gases and the production of iron compounds occur through chemical reactions described by the following equations:



The first chemical equation shows that four bound water molecules within the crystal are evaporated with increasing temperature. Therefore, the theoretical weight loss due to the evaporation of  $4\text{H}_2\text{O}$  is calculated to be 14.5% ( $=4 \times 18.02/497.92$ ), which is very close to the experimental weight loss of 14.9% in the range of 300–400 K. According to the second step of the reaction, the elimination of the remaining  $\text{H}_2\text{O}$  molecule, the evolution of  $4\text{H}_2\text{CO}$  and  $2\text{CO}$  gases, and the generation of iron carbonate ( $2\text{FeCO}_3$ ) occur in the range of 400–720 K. Here, the weight loss is calculated to be 39.0% ( $=(18.02+4 \times 30.03+2 \times 28.01)/497.92$ ). This value is also very close to the experimental weight loss of 38.6%. The weight losses due to the evolution of  $4\text{H}_2\text{CO}$  and  $2\text{CO}$  gases may be associated with the DTG peaks at 629 and 649 K which indicate two different types of decomposition behavior. According to the last equation, the evolution of  $(5/3)\text{O}_2$  gas occurs in the range of 720–1060 K, and therefore the weight loss is calculated to be 10.7% ( $=(5/3) \times 32.00/497.92$ ). This value is approximately 3% larger than the experimental weight loss of 7.8%. This difference may be mainly caused by the increase in the sample weight owing to the incorporation of nitrogen atoms (delivered by the gas flow) into the sample. Since the slight increase of 1.3% (shown in Fig. 3) is observed on the TG curve in the temperature range of 1060–1320 K, a similar increase is anticipated to occur in the range of 720–1060 K. The experimental weight loss observed in this range might become relatively smaller in magnitude owing to the incorporation of nitrogen atoms; consequently, the difference between the experimental and theoretical values becomes larger. The theoretical calculation results based on the chemical reactions for  $\text{FeC}_4\text{H}_4\text{O}_6 \cdot 2.5\text{H}_2\text{O}$  are almost consistent with the experimental weight losses, as shown in Table 5.

After heating up to 1320 K for the TG-DTA measurements, we found that a black residue was present in the vessel. The chemical reactions described above indicate that triiron tetraoxide  $\text{Fe}_3\text{O}_4$  and carbon are produced by the thermal decomposition of  $\text{FeC}_4\text{H}_4\text{O}_6 \cdot 2.5\text{H}_2\text{O}$ . It is well known that  $\text{Fe}_3\text{O}_4$  reacts readily with oxygen to form diiron trioxide  $\text{Fe}_2\text{O}_3$  which is reddish-brown in color. However, the oxidation reaction from  $\text{Fe}_3\text{O}_4$  to  $\text{Fe}_2\text{O}_3$  does not occur because the sample was kept under a nitrogen atmosphere during the measurements. The color of the residue is different from that of  $\text{Fe}_2\text{O}_3$ . Therefore, the black residue left in the vessel may be composed of  $\text{Fe}_3\text{O}_4$  and carbon.

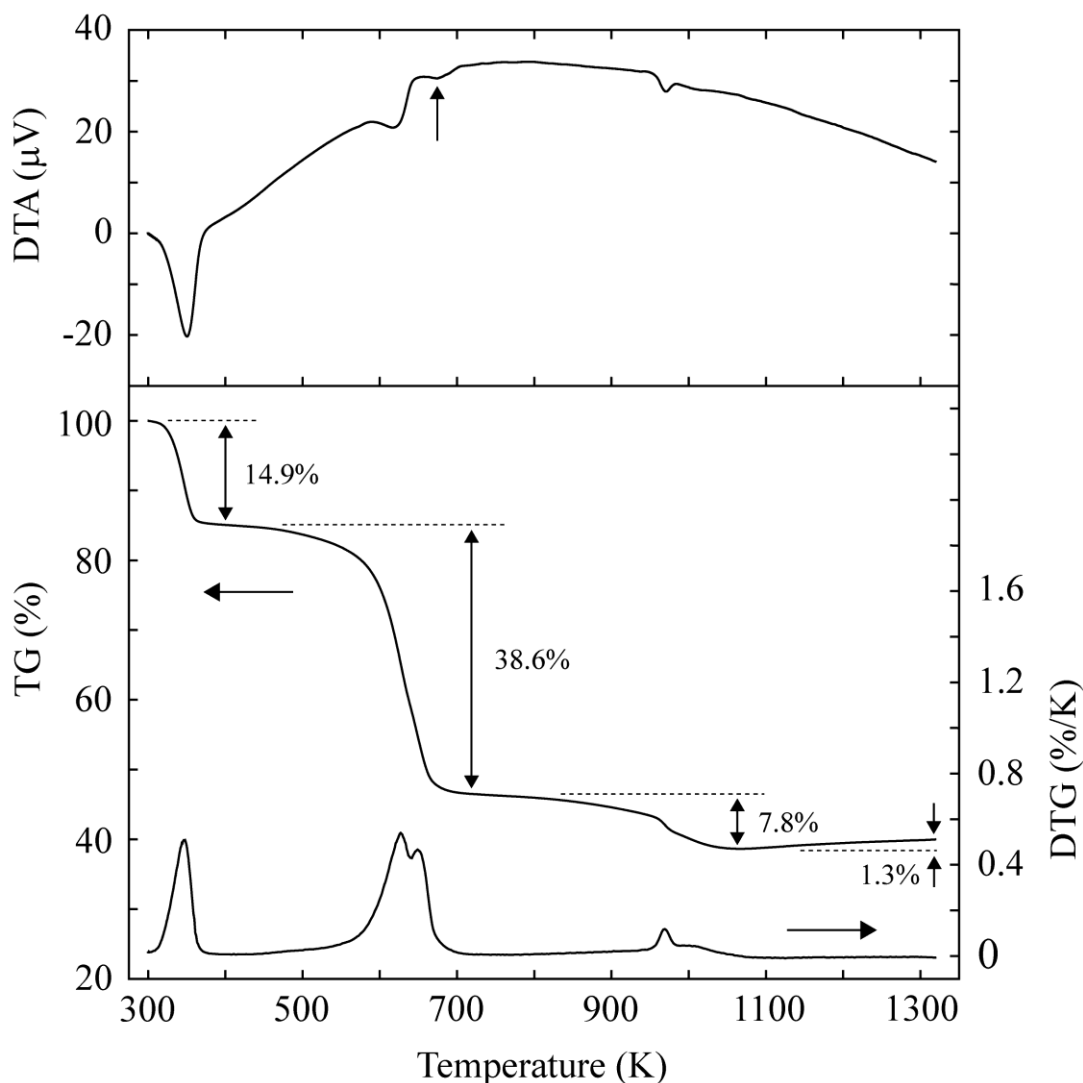


Figure 3. TG, DTG, and DTA curves for  $\text{FeC}_4\text{H}_4\text{O}_6 \cdot 2.5\text{H}_2\text{O}$  on heating

#### 4. Summary

Single crystals of iron(II) tartrate hemi-pentahydrate,  $\text{FeC}_4\text{H}_4\text{O}_6 \cdot 2.5\text{H}_2\text{O}$ , were grown at room temperature by the gel method using silica gels. The thermal properties and crystal structure of the single crystals were studied by DSC, TG-DTA, and X-ray diffraction methods. The structure at room temperature was orthorhombic with space group  $P2_12_12_1$ , and consisted of slightly distorted  $\text{FeO}_6$  octahedra,  $\text{C}_4\text{H}_4\text{O}_6$  and  $\text{H}_2\text{O}$  molecules,  $\text{C}_4\text{H}_4\text{O}_6\text{-Fe-C}_4\text{H}_4\text{O}_6$  chains running along the  $c$ -axis, and  $\text{O-H}\cdots\text{O}$  hydrogen-bonded frameworks between adjacent molecules in the  $ab$ -planes. No phase transition was found in the temperature range of 100–315 K, and the significant weight losses due to the thermal decomposition were observed in the temperature range of 300–1060 K. The chemical equations illustrating the decomposition reaction of the crystal were presented, with corresponding temperature ranges. We suggested that the weight losses are caused by the evaporation of bound  $\text{H}_2\text{O}$  molecules and the evolution of  $\text{H}_2\text{CO}$ ,  $\text{CO}$ , and  $\text{O}_2$  gases from  $\text{C}_4\text{H}_4\text{O}_6$  molecules, and that the black residue left in the vessel after decomposition consists of  $\text{Fe}_3\text{O}_4$  and carbon.

#### References

- Abdel-Kader, M. M., El-Kabbany, F., Taha, S., Abosehly, A. M., Tahoon, K. K., & El-Sharkawy, A. A. (1991). Thermal and electrical properties of ammonium tartrate. *J. Phys. Chem. Solids*, 52(5), 655-658. [https://doi.org/10.1016/0022-3697\(91\)90163-T](https://doi.org/10.1016/0022-3697(91)90163-T)
- Bootsma, G. A., & Schoone, J. C. (1967). Crystal structures of mesotartaric acid. *Acta Crystallogr.*, 22(4), 522–532. <https://doi.org/10.1107/S0365110X67001070>

- Burla, M. C., Caliandro, R., Carrozzini, B., Cascarano, G. L., Cuocci, C., Giacovazzo, C., ... & Polidori, G. (2015). Crystal structure determination and refinement via SIR2014. *J. Appl. Crystallogr.*, 48(1), 306-309. <https://doi.org/10.1107/S1600576715001132>
- Desai, C. C., & Patel, A. H. (1988). Crystal data for ferroelectric  $\text{RbHC}_4\text{H}_4\text{O}_6$  and  $\text{NH}_4\text{HC}_4\text{H}_4\text{O}_6$  crystals. *J. Mater. Sci. Lett.*, 7(4), 371-373. <https://doi.org/10.1007/BF01730747>
- Dhikale, M. D., Shitole, S. J., Nahire, S. B., & Chavan, A. R. (2019). Electric conductivity study of silica gel grown pure and Cu doped Fe tartrate crystals. *J. Gujarat Res. Society*, 21(14), 1574-1581. <http://www.gujaratresearchsociety.in/index.php/JGRS/article/view/2286>
- Farrugia, L. J. (2012). WinGX and ORTEP for Windows: an update. *J. Appl. Crystallogr.*, 45(4), 849-854. <https://doi.org/10.1107/S0021889812029111>
- Firdous, A., Quasim, I., Ahmad, M. M., & Kotru, P. N. (2010). Dielectric and thermal studies on gel grown strontium tartrate pentahydrate crystals. *Bull. Mater. Sci.*, 33(4), 377-382. <https://doi.org/10.1007/s12034-010-0057-1>
- Fukami, T., Tahara, S., Yasuda, C., & Nakasone, K. (2016). Structural refinements and thermal properties of L(+)-tartaric, D(-)-tartaric, and monohydrate racemic tartaric acid. *Inter. J. Chem.*, 8(2), 9-21. <https://doi.org/10.5539/ijc.v8n2p9>
- Fukami, T., & Tahara, S. (2018). Structural and thermal studies on racemic  $\text{PbC}_4\text{H}_4\text{O}_6 \cdot 2\text{H}_2\text{O}$  single crystal. *Chem. Sci. Int. J.*, 25(1), 45004 (1-9). <https://doi.org/10.9734/CSJI/2018/45004>
- Fukami, T., & Tahara, S. (2020). Crystal structures and thermal properties of L- $\text{MnC}_4\text{H}_4\text{O}_6 \cdot 2\text{H}_2\text{O}$  and DL- $\text{MnC}_4\text{H}_4\text{O}_6 \cdot 2\text{H}_2\text{O}$ . *Inter. J. Chem.*, 12(1), 78-88. <https://doi.org/10.5539/ijc.v12n1p78>
- Fukami, T., & Tahara, S. (2021). Structural and thermal investigations of L- $\text{CuC}_4\text{H}_4\text{O}_6 \cdot 3\text{H}_2\text{O}$  and DL- $\text{CuC}_4\text{H}_4\text{O}_6 \cdot 2\text{H}_2\text{O}$  Single Crystals. *Inter. J. Chem.*, 13(1), 38-49. <https://doi.org/10.5539/ijc.v13n1p38>
- Joseph, S., Joshi, H. S., & Joshi, M. J. (1997). Infrared spectroscopic and thermal studies of gel grown spherulitic crystals of iron tartrate. *Cryst. Res. Technol.*, 32(2), 339-346. <https://doi.org/10.1002/crat.2170320218>
- Kachi, S. (1974). Crystal growth in gel. *J. Crystallogr. Soc. Japan*, 16(1), 115-119 [in Japanese]. <https://doi.org/10.5940/jcrsj.16.115>
- Labutina, M. L., Marychev, M. O., Portnov, V. N., Somov, N. V., & Chuprunov, E. V. (2011). Second-order nonlinear susceptibilities of the crystals of some metal tartrates. *Crystallogr. Rep.*, 56(1), 72-74. <https://doi.org/10.1134/S1063774510061082>
- Mathivanan, V., & Haris, M. (2013). Characterization of pure and copper-doped iron tartrate crystals grown in silica gel. *Pramana*, 81(1), 177-187. <https://doi.org/10.1007/s12043-013-0564-x>
- Sheldrick, G. M. (2015). Crystal structure refinement with SHELXL. *Acta Crystallogr.*, C71(1), 3-8. <https://doi.org/10.1107/S2053229614024218>
- Song, Q. B., Teng, M. Y., Dong, Y., Ma, C. A., & Sun, J. (2006). (2S,3S)-2,3-Dihydroxy-succinic acid monohydrate. *Acta Crystallogr.*, E62(8), o3378-o3379. <https://doi.org/10.1107/S1600536806021738>
- Torres, M. E., Peraza, J., Yanes, A. C., López, T., Stockel, J., López, D. M., Solans, X., Bocanegra, E., & Silgo, C. G. (2002). Electrical conductivity of doped and undoped calcium tartrate. *J. Phys. Chem. Solids*, 63(4), 695-698. [https://doi.org/10.1016/S0022-3697\(01\)00216-5](https://doi.org/10.1016/S0022-3697(01)00216-5)
- Venkataraman, A., Mukhedkar, V. A., & Mukhedkar, A. J. (1989). Synthesis of  $\gamma\text{-Fe}_2\text{O}_3$  by thermal decomposition of  $\text{FeC}_4\text{H}_4\text{O}_6 \cdot 2.5\text{H}_2\text{O}$ . *J. Therm. Analysis*, 35, 2115-2124. <https://doi.org/10.1007/BF01911876>

## Copyrights

Copyright for this article is retained by the author(s), with first publication rights granted to the journal.

This is an open-access article distributed under the terms and conditions of the Creative Commons Attribution license (<http://creativecommons.org/licenses/by/4.0/>).